Infrared quantum cutting conversion luminescence of Tb(0.7)Yb(3):FOV*

Chen Xiao-Bo(陈晓波)[a)†], Kang Dong-Guo(康洞国)[b)], Li Song(李 崧)[a)], Wen Lei(温 磊)[c)], Yu Chun-Lei(于春雷)[c)], Hu Li-Li(胡丽丽)[c)], and Zhou Jing(周 静)[a)]

[a)] *Nuclear Science & Technology College and Analytical Testing Center, Applied Optics Beijing Area Major Laboratory, Beijing Normal University, Beijing* 100875, *China*

[b)] *Beijing Institute of Applied Physics and Computational Mathematics, Beijing* 100088, *China*

[c)] *Shanghai Institute of Optics and Fine Mechanics, Chinese Academy of Sciences, Shanghai* 201800, *China*

(Received 3 June 2010; revised manuscript received 1 August 2010)

The infrared quantum cutting of oxyfluoride nanophase vitroceramics Tb(0.7)Yb(3):FOV has been studied in the present paper. The actual quantum cutting efficiency formula calculated from integral fluorescence intensity is extended to the case of Tb(0.7)Yb(3):FOV. The visible and the infrared fluorescence spectra and their integral fluorescence intensities are measured from static fluorescence experiment. Lifetime curve is measured from dynamic fluorescence experiment. It is found that the total actual quantum cutting efficiency η of the excited $^5D_4$ level is about 93.7%, and that of excited ($^5D_3$, $^5G_6$) levels is 93.5%. It is also found that the total theoretical quantum cutting efficiency upper limit $\eta_{x\%Yb}$ of the 485.5 nm excited $^5D_4$ level is about 121.7%, and that of 378.5 nm excited ($^5D_3$, $^5G_6$) levels is 137.2%.

Keywords: infrared quantum cutting, solar cell, oxyfluoride nanophase vitroceramics Tb(0.7)Yb(3):FOV

PACS: 78.55.-m, 78.55.–a, 78.30.–j **DOI:** 10.1088/1674-1056/20/2/027801

1. Introduction

One of the important tasks in luminescence material research nowadays is to develop new phosphors for conversion from the visible to infrared spectral region.[1−7] It is urgently needed to convert the visible and the violet radiation from solar spectrum into infrared light in solar cell application with a higher efficiency and stability.[1,2] Since the visible quantum cutting in Eu^{3+}–Gd^{3+} material was reported by Wegh *et al.* in Science,[2] the quantum cutting phenomena have been widely recognized to have useful applications.[1−13] One of their applications is the vacuum-UV-to-visible quantum cutting used for the noble gas discharge tube lamp source.[1,2,10−12] Another application is the visible-to-infrared quantum cutting used for the solar cells.[7,8,14−16] From 2007, more than twenty high quality articles dealing with infrared quantum cutting field have been published in a series of top journals.[2,7−10,14−17] It means that the infrared quantum cutting research has become an international hot field already. In fact, in recent years we have been facing the increasingly serious problems of reduction in fossil energy and environmental pollution. Therefore, it is valuable to improve the utilization of solar energy by quantum cutting to enhance the conversion efficiency of solar cells.[7−17] On the other hand, the quantum cutting downconversion luminescence is the further development for upcoversion research.[10−30]

So far, the most perfect development in solar cells should be in silicon solar cells, which have been produced in many countries. New theory, materials, techniques, designs, and products of solar cells have been increasingly improved. The development of germanium solar cells is more rapid as a new type of solar cell with a narrow band-gap width,[1−7] which has been used in germanium, silicon-germanium and cascade three-junction solar cells.[3,4] The germanium solar cell has its proper advantages because the small band-gap width of germanium is 0.785 eV.[1−7] However, the thermalization of charge carries, resulting from the absorption of high energy photons, is one of the ma-

*Project supported by the National Natural Science Foundation of China (Grant No. 10674019).

†Corresponding author. E-mail: chen78xb@sina.com, xbchen@bnu.edu.cn

© 2011 Chinese Physical Society and IOP Publishing Ltd

jor loss mechanisms by which collected energy is underutilized as in a conventional solar cell.[7−10] Quantum cutting method can reduce these energy losses. Each energetic photon can result in two or more infrared photons. Therefore the efficiency of solar cell is enhanced greatly. Meanwhile the problem of device overheat is solved. So the quantum cutting solar cell is economically more competitive and feasible.[7−10,28]

The infrared quantum cutting of oxyfluoride nanophase vitroceramics Tb(0.7)Yb(3):FOV is studied in the present paper. The accurate experiment, the relative theoretical calculation and the analysis have been performed.

2. Sample and equipment

The oxyfluoride glass samples are made from SiO_2, PbF_2, ZnF_2, LuF_3, YbF_3, and TbF_3. The nanophase oxyfluoride vitroceramic is obtained by 7-hour annealing at about the glass transition temperature T_g = 389 °C.[7,8,14] The samples used in our experiments are oxyfluoride nanophase vitroceramics (FOV) which are (i) Tb(0.7)Yb(3):FOV, (ii) Tb(0.7):FOV. The Tb(0.7)Yb(3):FOV is doped with Tb^{3+} and Yb^{3+} ions at the concentrations of 0.7 mol% and 3 mol% respectively.

The experimental equipment used is the Fluorescence Spectrometer F900 made by Edinburgh Instruments Ltd Company. The detector used for infrared wavelength range is Ge photocell which has a good sensitivity in a wavelength range from 800 nm to 1700 nm. The monochromator is a high-precision monochromator with a resolution of 0.05 nm. The direction of the excitation light is perpendicular to the direction of receiving fluorescence. And all of the experimental signal curves have been calibrated. Part fluorescence spectra are measured by using the Fluorolog-Tau-3 fluorescence spectrophotometer (JY-ISA) so as to obtain a very good signal-to-noise ratio.[23]

3. Experimental results of quantum cutting

3.1. Measured results of excitation spectra

The visible excitation spectra of 543.0-nm $^5D_4 \rightarrow {}^7F_5$ fluorescence, 582.0-nm $^5D_4 \rightarrow {}^7F_4$ fluorescence and 620.0-nm $^5D_4 \rightarrow {}^7F_3$ fluorescence of Tb^{3+} ion of Tb(0.7)Yb(3):FOV were measured as shown in Fig. 1(a). The infrared excitation spectrum of $^2F_{5/2} \rightarrow {}^2F_{7/2}$ 973.0-nm fluorescence of Yb^{3+} ion of Tb(0.7)Yb(3):FOV is also measured as shown in Fig. 1(b). It can be found from Fig. 1 that there are several obvious excitation spectrum peaks positioned at 378.5, 368.5, 358.0, 485.5, 352.0, and 341.5.0 nm separately. It is easy to recognize these excitation peaks corresponding to the absorptions of energy levels of ($^5D_3$, $^5G_6$), $^5L_{10}$, $^5G_5$, $^5D_4$, ($^5G_4$, $^5L_9$), and ($^5L_8$, $^5L_7$).

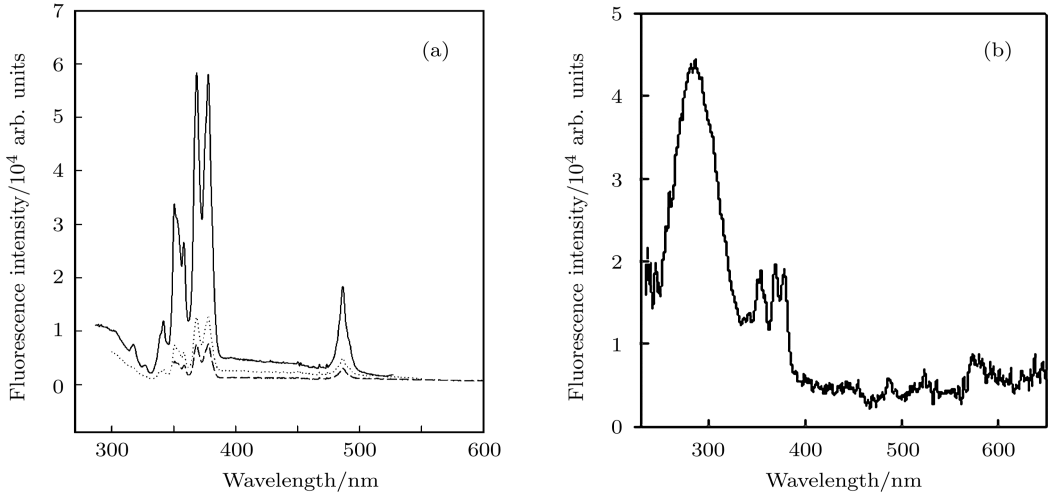


Fig. 1. Visible fluorescence excitation spectra of Tb(0.7)Yb(3.0):FOV, received at 543.0-nm (solid line), 582.0-nm (dot line) and 620.0-nm (dash line) fluorescence wavelength positions (a), and infrared fluorescence excitation spectrum of Tb(0.7)Yb(3.0):FOV, received at 973.0-nm fluorescence wavelength position (b).

3.2. Experimental results of quantum cutting emission spectra

The visible fluorescence emission spectra of Tb(0.7)Yb(3):FOV are measured. The excitation peaks 378.5 nm and 485.5 nm of Tb(0.7)Yb(3):FOV are selected to excite the Tb(0.7)Yb(3):FOV so as to obtain its visible fluorescence emission spectra as shown in Fig. 2(a). It is found from the experiment that there are a number of visible fluorescence lines positioned at 485.5, 543.0, 582.0, and 620.0 nm respectively. It is easy to recognize that these fluorescence lines are from the $^5D_4 \rightarrow {}^7F_6$, $^5D_4 \rightarrow {}^7F_5$, $^5D_4 \rightarrow {}^7F_4$, and $^5D_4 \rightarrow {}^7F_3$ fluorescence transitions respectively. Their calibrated fluorescence integral intensities are calculated carefully from the measured fluorescence spectra. All measured visible fluorescence transitions and their calibrated fluorescence integral intensities are listed in Table 1.

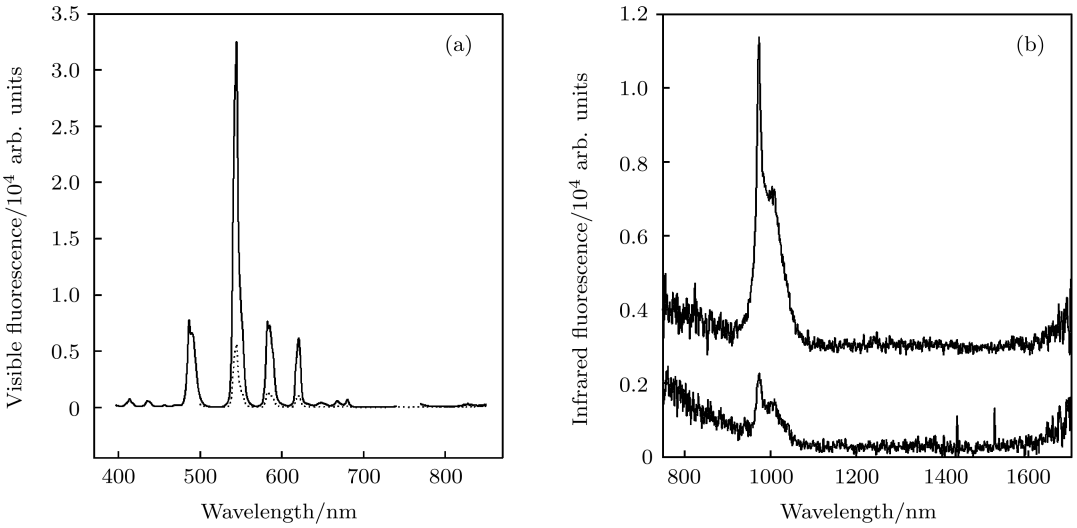


Fig. 2. Visible fluorescence emission spectra of Tb(0.7)Yb(3.0):FOV when ($^5D_3$, $^5G_6$) and $^5D_4$ levels are excited by 378.5 nm (solid line) and 485.5 nm (dot line) respectively (a), and infrared fluorescence emission spectra of Tb(0.7)Yb(3.0):FOV when ($^5D_3$, $^5G_6$) and $^5D_4$ levels are excited by 378.5 nm (upper) and 485.5 nm (lower) respectively.

Table 1. Integral calibrated fluorescence intensities of 485.5, 543.0, 582.0, 620.0, and 973.0 nm fluorescence lines and the total actual quantum cutting efficiency η of Tb(0.7)Yb(3):FOV when $^5D_4$, and ($^5D_3$, $^5G_6$) levels are excited by 485.5-nm, and 378.5-nm light respectively.

excitation wavelength/nm	the integral calibrated fluorescence intensity /arb. uints					surplus sum	ratio	η/%
	485.5/nm	543.0/nm	582.0/nm	620.0/nm	973.0/nm			
485.5	14577	42452	11370	6693	65627	75092	0.8738	93.7
378.5	77833	226671	60335	32548	345605	397387	0.8697	93.5

Then, the infrared fluorescence emission spectra of Tb(0.7)Yb(3):FOV are also measured. Likewise, the excitation peaks 378.5 nm and 485.5 nm of Tb(0.7)Yb(3):FOV are selected to excite the Tb(0.7)Yb(3):FOV so as to obtain its infrared fluorescence emission spectra as shown in Fig. 2(b). It is found that there is one infrared fluorescence line positioned at 973 nm, which can be recognized to be due to the $^2F_{5/2} \rightarrow {}^2F_{7/2}$ 973.0-nm infrared fluorescence transition of Yb^{3+} ion. The measured infrared fluorescence transition and their calibrated fluorescence integral intensities are also listed in Table 1. Figure 2(b) shows that the first line gives the 750–1700 nm infrared fluorescence spectrum when $^5D_4$ level is excited by 485.5-nm light, and that the second line gives the 750–1700 nm infrared fluorescence spectrum when ($^5D_3$, $^5G_6$) level is excited by 378.5-nm light. All measured conditions are normalized. And all measured curves and data in Fig. 2 and Table 1 are calibrated, whose relative intensities can be compared directly already.

3.3. Experimental results of quantum cutting fluorescence lifetime

The visible 543.0-nm fluorescence lifetimes of Tb(0.7)Yb(3):FOV and Tb(0.7):FOV are measured. The excitation peaks 378.5 nm and 485.5 nm of Tb^{3+} ion are selected to excite the Tb(0.7)Yb(3):FOV and Tb(0.7):FOV so as to obtain their visible 543.0-nm fluorescence lifetime curves as shown in Figs. 3 and 4. Their 543.0-nm fluorescence lifetime values are calculated from experiment lifetime curves, which are all listed in Table 2. Their structural diagrams of energy level of Tb^{3+} ion and Yb^{3+} ion are shown in Fig. 5.

Table 2. The 543.0-nm fluorescence lifetimes of Tb(0.7):FOV and Tb(0.7)Yb(3.0):FOV excited by 485.5-nm and 378.5-nm light respectively, and the values of their total theoretical quantum cutting efficiency upper limit $\eta_{x\%\mathrm{Yb}}$ of Tb(0.7)Yb(3):FOV when the $^5\mathrm{D}_4$, and ($^5\mathrm{D}_3$, $^5\mathrm{G}_6$) levels are excited by 485.5-nm and 378.5-nm light respectively.

excitation wavelength/nm	lifetime of Tb(0.7):FOV/ms	lifetime of Tb(0.7)Yb(3.0):FOV/ms	$\eta_{\mathrm{tr},x\%\mathrm{Yb}}$/%	$\eta_{x\%\mathrm{Yb}}$/%
485.5 nm	2.54	2.05	21.73	121.73
378.5 nm	2.75	2.07	37.25	1 37.25

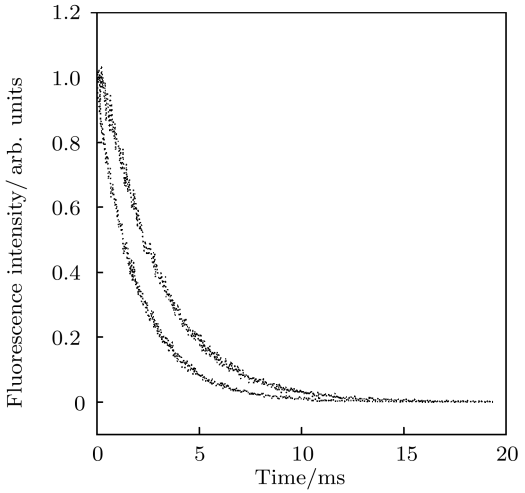


Fig. 3. The 543.0-nm fluorescence lifetime curves of Tb(0.7):FOV (upper) and Tb(0.7)Yb(3.0):FOV (lower) when they are excited by 378.5-nm light respectively.

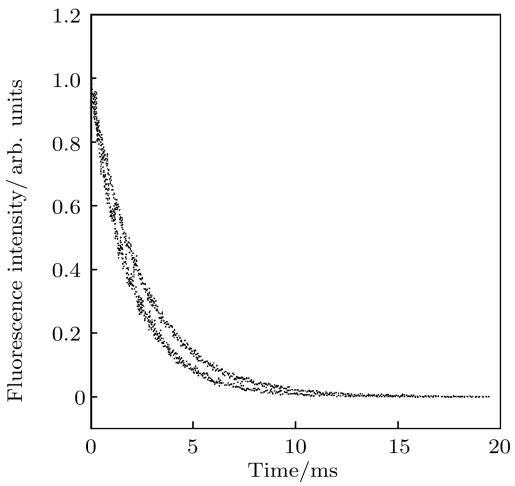


Fig. 4. The 543.0-nm fluorescence lifetime curve of (a) Tb(0.7):FOV (upper) and (b) Tb(0.7)Yb(3.0):FOV (lower) when they are excited by 485.5-nm light respectively.

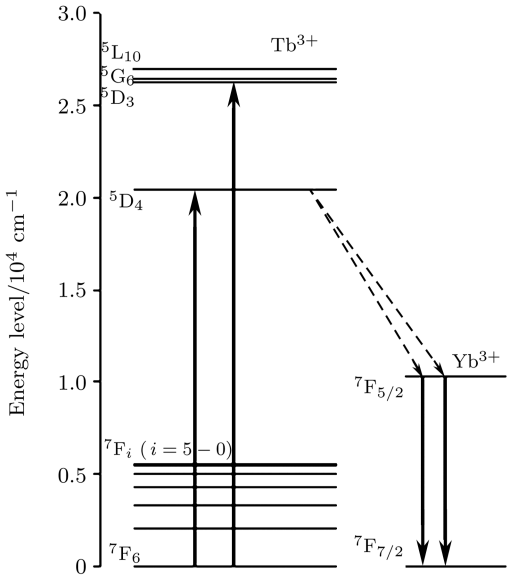


Fig. 5. Structural diagram of energy levels of Tb^{3+} ion and Yb^{3+} ion.

4. Quantum cutting efficiency calculated from fluorescence lifetime

According to the well-known infrared quantum cutting of Tb^{3+}–Yb^{3+} system, the theoretical transfer luminous efficiency of $^2\mathrm{F}_{5/2}$ level caused by cross-relaxation energy transfer is determined from the following formula in which the fluorescence lifetime curve is used:[7−10,12−15]

$$\eta_{\mathrm{tr},x\%\mathrm{Yb}} = 1 - \frac{\int I_{x\%\mathrm{Yb}}\,\mathrm{d}t}{\int I_{0\%\mathrm{Yb}}\,\mathrm{d}t}, \tag{1}$$

where I denotes the intensity and x%Yb refers to the Yb^{3+} concentration. The total theoretical quantum cutting efficiency $\eta_{x\%\mathrm{Yb}}$ can be expressed as follows:

$$\begin{aligned}\eta_{x\%\mathrm{Yb}} &= \eta_{\mathrm{rTb}}(1-\eta_{\mathrm{tr},x\%\mathrm{Yb}}) + 2\eta_{\mathrm{tr},x\%\mathrm{Yb}} \\ &= 1 + \eta_{\mathrm{tr},x\%\mathrm{Yb}},\end{aligned} \tag{2}$$

where the fluorescence quantum efficiency for the Tb^{3+} ions, η_{rTb}, is set to 1.[7−10,12−15]

It is needed to emphasize that the authors in Ref. [10] and others have pointed out that formulas (1) and (2) yield the theoretical upper limit values for the quantum efficiency $\eta_{x\%\mathrm{Yb}}$, but the actual quantum efficiency is strongly reduced by concentration quenching, etc.[10]

We also calculated the total theoretical quantum cutting efficiency $\eta_{x\%\mathrm{Yb}}$ from formulas (1) and (2) from the measured lifetime curves, which are shown

in Figs. 3 and 4. The calculated results are listed in Table 2. It can be seen from Table 2 that the total theoretical quantum cutting efficiency $\eta_{x\%\mathrm{Yb}}$ of the 485.5-nm excited $^5\mathrm{D}_4$ level is about 121.7%, and that of 378.5-nm excited ($^5\mathrm{D}_3$, $^5\mathrm{G}_6$) levels is 137.2%.

5. Quantum cutting efficiency calculated from integral fluorescence intensity

According to the visible quantum cutting of Eu^{3+}–Gd^{3+} system, the actual luminous efficiency of $^5\mathrm{D}_0$ level caused by cross-relaxation energy transfer is determined from the following formula[1,2]

$$\frac{P_{\mathrm{CR}}}{P_{\mathrm{CR}}+P_{\mathrm{DT}}} = \frac{R\,(^5\mathrm{D}_0/^5\mathrm{D}_{1,2,3})_{^6\mathrm{G_J}} - R\,(^5\mathrm{D}_0/^5\mathrm{D}_{1,2,3})_{^6\mathrm{I_J}}}{R\,(^5\mathrm{D}_0/^5\mathrm{D}_{1,2,3})_{^6\mathrm{I_J}}+1}, \quad (3)$$

where P_{CR} is the rate of cross-relaxation energy transfer, P_{DT} is the energy transfer rate directly from Gd^{3+} to Eu^{3+}, $R\,(^5\mathrm{D}_0/^5\mathrm{D}_{1,2,3})$ is the integral fluorescence emission intensity ratio between $^5\mathrm{D}_0$ and $^5\mathrm{D}_{1,2,3}$.

The above formula determined by the integral fluorescence intensity ratio is most direct and intuitive, so it is a good way to use well-known formula (3) to calculate quantum cutting efficiency.

As for the calculation of quantum cutting phenomena of Tb(0.7)Yb(3):FOV discussed in the present paper, we can use a new formula which is obtained by extending formula (3) to the quantum cutting efficiency calculation of Tb^{3+} and Yb^{3+} codoped system.

The formula for calculating the actual quantum cutting luminous efficiency of $^2\mathrm{F}_{5/2}$ level of Yb^{3+} ion, caused by cross-relaxation energy transfer, can be expressed as follows:[11,12]

$$\frac{P_{\mathrm{CR}}}{P_{\mathrm{CR}}+P_{\mathrm{DT}}} = \frac{R\,(^2\mathrm{F}_{5/2}/\mathrm{rest})_{\mathrm{Tb}^{3+}} - R\,(^2\mathrm{F}_{5/2}/\mathrm{rest})_{\mathrm{Yb}^{3+}}}{R\,(^2\mathrm{F}_{5/2}/\mathrm{rest})_{\mathrm{Yb}^{3+}}+1}, \quad (4)$$

where $R\,(^2\mathrm{F}_{5/2}/\mathrm{rest})$ represents the ratio of the integral fluorescence intensity of $^2\mathrm{F}_{5/2}$ level of Yb^{3+} ions to all the other integral fluorescence intensities including $^5\mathrm{D}_4$ and $^5\mathrm{D}_3$ levels of Tb^{3+}. The subscript indicates the excited level or excited ion.

Thus, the total actual quantum cutting efficiency η can be expressed as follows:

$$\begin{aligned}\eta(^2\mathrm{F}_{5/2}) &= 1+\frac{P_{\mathrm{CR}}}{P_{\mathrm{CR}}+P_{\mathrm{DT}}} \\ &= 1+\frac{R\,[(^2\mathrm{F}_{5/2})/\mathrm{rest}]_{\mathrm{Tb}^{3+}} - R\,[(^2\mathrm{F}_{5/2})/\mathrm{rest}]_{\mathrm{Yb}^{3+}}}{R\,[(^2\mathrm{F}_{5/2})/\mathrm{rest})]_{\mathrm{Yb}^{3+}}+1} \\ &= \frac{R\,[(^2\mathrm{F}_{5/2})/\mathrm{rest}]_{\mathrm{Tb}^{3+}}+1}{R\,[(^2\mathrm{F}_{5/2})/\mathrm{rest}]_{\mathrm{Yb}^{3+}}+1}. \end{aligned} \quad (5)$$

Because activator Yb^{3+} has only one excited level $^2\mathrm{F}_{5/2}$ level, other luminescent level, "rest", is just $^2\mathrm{F}_{5/2}$ level itself when Yb^{3+} ion is excited. Therefore, we have

$$R\,[(^2\mathrm{F}_{5/2})/\mathrm{rest}]_{\mathrm{Yb}^{3+}} = 1, \quad (6)$$

$$\begin{aligned}\eta(^2\mathrm{F}_{5/2}) &= \frac{R\,[(^2\mathrm{F}_{5/2})/\mathrm{rest}]_{\mathrm{Tb}^{3+}}+1}{R\,[(^2\mathrm{F}_{5/2})/\mathrm{rest}]_{\mathrm{Yb}^{3+}}+1} \\ &= \frac{R\,[(^2\mathrm{F}_{5/2})/\mathrm{rest}]_{\mathrm{Tb}^{3+}}+1}{1+1} \\ &= \frac{R\,[(^2\mathrm{F}_{5/2})/\mathrm{rest}]_{\mathrm{Tb}^{3+}}+1}{2}. \end{aligned} \quad (7)$$

The fluorescence spectra from visible to near-infrared regions of the excited levels, 485.5-nm $^5\mathrm{D}_4$ and 378.5-nm ($^5\mathrm{D}_3$, $^5\mathrm{G}_6$) levels, are measured. The integral fluorescence intensities of all the fluorescence lines are list in Table 1. The total actual quantum cutting efficiency η can be calculated easily from the above formulas (3)–(7), and the calculations are also listed in Table 1. It can be seen from Table 1 that the total actual quantum cutting efficiency η of the excited $^5\mathrm{D}_4$ level is about 93.7%, and that of excited ($^5\mathrm{D}_3$, $^5\mathrm{G}_6$) levels is 93.5% respectively.

6. Analysis

It is well known that the energy transfer theory has been developed by Forster,[25] Dexter[26] and Kushida.[27] These theories are based on several interaction models between donor and acceptor, just like dipolar–dipolar interaction or wave function overlap exchange interaction. What is in common lies in the fact that they both require resonance between the transitions of donor and acceptor. That is to say, the cross-energy transfer can be strong only when the emission spectrum of donor and the excitation spectrum of acceptor is overlaped. The

whole concept of quantum cutting is based on this theory.[1,2,7−10,13,22−27]

If the overlap between donor emission and acceptor absorption is absent, the second-order downconversion may become a dominant relaxation process. The Tb^{3+}–Yb^{3+} codoped material is just a typical second-order downconversion quantum cutting system. It can be seen from the structural diagram (Fig. 5) of energy levels of Tb^{3+} ion and Yb^{3+} ion. In this process a Tb^{3+} donor excites two Yb^{3+}acceptors simultaneously. The resonance condition is fulfilled because the sum of the energies of the absorption transitions of two Yb^{3+}acceptor centres equals the energy of the emission of one donor Tb^{3+}. And it is obvious that the lifetime of $^5D_4$ level of Tb^{3+} ion is very long because the energy gap between the $^5D_4$ level and the lower level is very large. Thus many Tb^{3+} donors can accumulate in the $^5D_4$ level to achieve effective second-order downconversion energy transfer.[10,18]

It can be seen from the experiment results (Figs. 2(a) and 2(b)) that the $^2F_{5/2}$ level of Yb^{3+} ion has strong luminescence, in which the fluorescence excited by 378.5 nm is larger than that excited by 485.5 nm because the absorption of the ($^5D_3$, $^5G_6$) is larger than that of $^5D_4$ level. It is interesting that the total actual quantum cutting efficiency η of the excited $^5D_4$ level is almost equal to that of excited ($^5D_3$, $^5G_6$) levels. It results from the fact that the luminescent energy level, when Tb^{3+} is excited by ($^5D_3$, $^5G_6$) level, is almost the same as that when Tb^{3+} is excited by $^5D_4$ level.

Meanwhile, it is clear that the total theoretical quantum cutting efficiency $\eta_{x\%\mathrm{Yb}}$ is larger than the total actual quantum cutting efficiency η, which results from concentration quenching and others.[10]

7. Conclusion

The infrared quantum cutting of nanophase oxyfluoride vitroceramics Tb(0.7)Yb(3):FOV has been studied in the present paper. From the measured visible and infrared fluorescence spectra and their integral fluorescence intensities, the actual quantum cutting efficiency η is calculated. It is found that the total actual quantum cutting efficiency η of the excited $^5D_4$ level is about 93.7%, and that of excited ($^5D_3$, $^5G_6$) levels is 93.5%. Through the measured lifetime curve, it is found that the total theoretical quantum cutting efficiency $\eta_{x\%\mathrm{Yb}}$ of the 485.5-nm excited $^5D_4$ level is about 121.7%, and that of 378.5-nm excited ($^5D_3$, $^5G_6$) levels is 137.2%. The relative physical processes are investigated and analysed.

Acknowledgement

The authors would like to thank Profs. Zhang Fei, Ding Hui-Fen, Yu Fei, He Chen-Jun, Wu Jin-Guang and Sun Ling of Peking University for their useful discussion and help.

References

[1] Yang G Z *National Natural Science Foundation of China* 1995 *Optical Physics* (Beijing: Science Press) (in Chinese)

[2] Wegh R T, Donker H, Oskam K D and Meijerink A 1999 *Science* **283** 663

[3] Bitnar B 2003 *Semicond. Sci. Technol.* **18** S221

[4] Matsui T, Ogata K, Isomura M and Kondo M 2006 *J. Non-crystalline Solids* **352** 1255

[5] Song Z F, Lian S R and Wang S K 1982 *Acta Phys. Sin.* **31** 772 (in Chinese)

[6] Zhou J J, Teng Y, Ye S, Xu X Q and Qiu J R 2010 *Opt. Express* **18** 21663

[7] Van der Ende B M, Aarts L and Meijerink A 2009 *Adv. Mater.* **21** 3073

[8] Chen D Q, Wang Y S, Yu Y L, Huang P and Weng F Y 2008 *Opt. Lett.* **33** 1884

[9] Richards B S 2006 *Solar Energy Materials & Solar Cells* **90** 1189

[10] Vergeer P, Vlugt T J H, Kox M H F, Hertog M I den, van der Eerden J P J M and Meijerink A 2005 *Phys. Rev.* B **71** 014119

[11] Lee T J, Luo L Y, Chen T M, Diau E W G, Cheng B M and Tung C Y 2006 *Appl. Phys. Lett.* **89** 131121

[12] Tzenga H Y, Cheng B M and Chen T M 2007 *J. Lumine.* **122–123** 917

[13] Carnall W T, Fieldd R and Rajnank K T 1968 *J. Chem. Phys.* **49** 4424

[14] Zhang Q Y and Huang X Y 2010 *Prog. Mater. Sci.* **55** 353

[15] Zhang Q Y, Yang C H and Pan Y X 2007 *Appl. Phys. Lett.* **90** 021107

[16] Wang N Y and Zhang L 2001 *Acta Phys. Sin.* **50** 693 (in Chinese)

[17] Ni P G, Chen H Y, Guo H L, Zhang Q and Zhang D Z 2003 *Appl. Phys. Lett.* **82** 373

[18] Chen X B, Song Z F and Sawanobori N 2001 *Chin. Phys.* **10** 565

[19] Kang X Y, Ji Y P and Jin Y J 2008 *Chin. Phys.* B **17** 1041

[20] Nie Y X, Yuan H T, Feng K C, Li C, He C J and Wang X J 2004 *Chin. Phys.* **13** 82

[21] Yang G J, Gong Q H and Wang K G 2000 *Acta Phys. Sin.* **49** 1485

[22] Xu X R and Shu M Z 2003 *Science of Luminescence and Luminescent Material* (Beijing: The Publishing Center of Material Science and Engineering) (in Chinese)

[23] Ni P G, Zhang S Z and Ji P W 2008 *Bulletin of National Natural Science Foundation of China* 2008/5 301 (in Chinese)

[24] Reisfeld R 1977 *Lasers and Excited States of Rare-Earth* (New York, Berlin, Heidelberg: Springer-Verlag)

[25] Forster T 1948 *Ann. Phys.* **2** 55

[26] Dexter D L 1957 *Phys. Rev.* **108** 630

[27] Kushida T 1973 *J. Phys. Soc. Jpn.* **34** 1318

[28] Li G J, Hou G F, Han X Y, Yuan Y J, Wei C C, Sun J, Zhao Y and Geng X H 2009 *Chin. Phys.* B **18** 1675

[29] Xiao S G and Yang X L 2002 *Chin. Phys.* **11** 188

[30] Wang E G, Guo Y, Zhang Y F, Oe T Z, Bao X Y, Tang Z, Zhang L X, Zhu W G, Niu Q, Qiu Z Q, Jia J F and Zhao Z X 2004 *Science* **306** 5703